Rigid N3O2-Pentadentate Ligand-Assisted Octacoordinate Mononuclear Ln(III) Complexes: Syntheses, Characterization, and Slow Magnetization Relaxation

Vaibhav Singh, Dhiraj Das, Srinivas Anga, J. P. Sutter, Vadapalli Chandrasekhar, Arun Kumar Bar

ACS OMEGA

http://pubs.acs.org/journal/acsodf

Article

Rigid N_3O_2-Pentadentate Ligand-Assisted Octacoordinate Mononuclear Ln(III) Complexes: Syntheses, Characterization, and Slow Magnetization Relaxation

Vaibhav Singh, Dhiraj Das, Srinivas Anga, Jean-Pascal Sutter,* Vadapalli Chandrasekhar,* and Arun Kumar Bar*

Cite This: *ACS Omega* 2022, 7, 25881−25890

Read Online

ACCESS | Metrics & More | Article Recommendations | Supporting Information

ABSTRACT: A series of air-stable mononuclear octacoordinate Ln(III) complexes, $[(L)Ln(TPPO)_3]OTf$ (Ln = Y (**1·Y**); Gd (**1·Gd**); Tb (**1·Tb**); Dy (**1·Dy**); Ho (**1·Ho**); and Er (**1·Er**)) and $[(L)Ln(TPPO)(NO_3)]$ (Ln = Y (**2·Y**) and Dy (**2·Dy**)), are synthesized employing a rigid N_3O_2-pentadentate chelating ligand as the basis ligand and meridional ancillary ligands (where H_2L = 2,6-diacetylpyridine *bis*-benzoylhydrazone, TPPO = triphenylphosphine oxide, and OTf^- = trifluoromethanesulfonate). All the complexes are synthesized under aerobic conditions and characterized comprehensively by spectroscopic and X-ray crystallographic techniques. Magnetic property investigation on the polycrystalline solid samples of **1·Ln** (Ln = Gd, Tb, Dy, Ho, and Er) and **2·Dy** are reported. A field-induced single-molecule magnet behavior was observed for the Dy derivatives. **1·Dy** exhibits the highest effective energy barrier of magnetization reversal, U_{eff}/k_B = 47 K under H_{dc} = 1 kOe among the complexes presented herein.

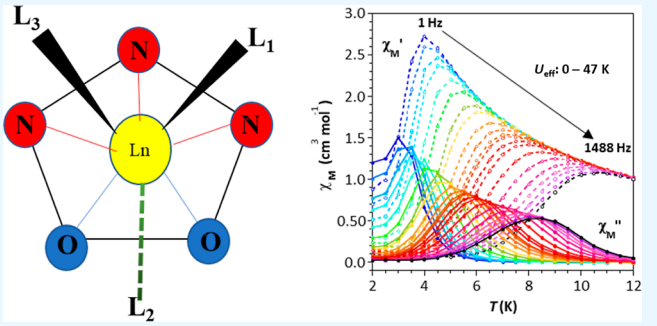

INTRODUCTION

A single-molecule magnet (SMM) is broadly referred to the paramagnetic metal complex exhibiting magnetization blocking and slow relaxation of magnetization below a critical temperature, generally known as the blocking temperature, T_B.[1,2] Due to the electronic spin-induced quantum magnetic states, SMMs inherit immense prospects in the high-impact modern technology such as high-density data storage, quantum computing, spintronics, bionics, multiferroics, and so forth.[3−8] However, the rational design and synthesis of potential SMMs are non-trivial. Since the discovery of the lanthanide (Ln) ion-based SMM behavior in phthalocyanine-sandwiched Ln(III) mononuclear complexes by Ishikawa et al.,[9,10] there has been an insurgence of research interest in the arena of molecule-based magnetism associated with Ln ions.[11−19] Notably, large spin ground state and high magnetic anisotropy originating from strong spin−orbit coupling bequeath the Ln complexes, especially the Dy(III)-analogues, with fascinating slow magnetization dynamics when the Ln ions are complexed with appropriate crystal field (CF) environments.[20−22] Recent advances reveal that the Ln-based complexes with low coordination numbers and high CF symmetry are expected to exhibit a promising SMM behavior, especially for the lanthanide ions having oblate electrostatic potential surfaces corresponding to their ground magnetic microstates.[18,23−31] However, it is worth mentioning that the Ln ions prefer large coordination numbers, commonly 8−10, and variable coordination geometry because of their large ionic size and highly shielded valance (4*f*) orbitals.[32,33] At the same time, a subtle change in the coordination environment can influence the SMM behavior significantly.[26,28−31,34−38] Therefore, having synthetic control over the inner coordination sphere with a desired CF topology is crucial in order for achieving potential SMMs rationally, especially for multinuclear SMMs.

Octacoordination is thermodynamically favorable for Ln ions due to the characteristic relative orientations of their valance (4*f*) orbitals, and hence, it is not a surprise why we observe octacoordinate Ln complexes most commonly.[18,22,39,40] Incidentally, the first-ever reported Ln-based SMMs are also octacoordinate complexes where the Ln(III) ions are sandwiched with two phthalocyanine N_4 pockets, leading to a nearly square-antiprism coordination geometry,[9] although the square prism CF symmetry is predicted to induce better SMM behavior for the Ln ions having oblate

Received: June 10, 2022
Accepted: June 28, 2022
Published: July 13, 2022

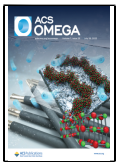

Scheme 1. Schematic Representation for the Syntheses of the Complexes 1·Ln (Ln = *Y*, Gd, Tb, Dy, Ho, and Er) and 2·Ln (Ln = *Y* and Dy)

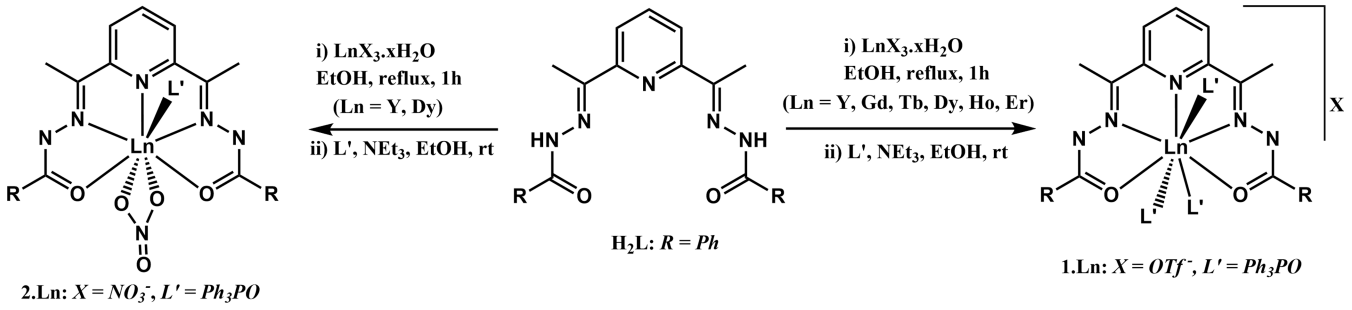

electrostatic potential surfaces corresponding to their ground magnetic microstates.[26] Nonetheless, fascinating SMM behaviors are observed in several pre-designed sandwiched-, half-sandwiched-, pseudo-sandwiched-, and multidecker Ln complexes with a square (anti)prism coordination geometry.[17,41−47] Notably, the 4*f*-orbitals of Ln ions are deeply buried, and consequently, their coordination bonds are relatively labile, which renders the inner sphere coordination geometry highly susceptible to the environments. Therefore, rigidification of the desired coordination geometry around the Ln ions is a challenge to the synthetic chemists.

Strong axial CF with higher symmetry brings forth better SMM properties for the Ln ions where the topology of the electrostatic potential surfaces corresponding to their ground magnetic microstates is oblate in nature.[26,39] However, except for a few examples where such Ln ions are kinetically stabilized under high axial symmetry, such as the D_{6h} symmetry,[48−50] most of the octacoordinate Ln complexes assume low symmetry, especially when the employed ligands bear lower denticity and higher flexibility. For such cases, post-synthetic modifications to tailor SMM properties are extremely difficult. Notably, association of appropriate metal ions into polynuclear systems with desired coordination geometries can result in large magnetic ground states and thereby promising SMMs. In our previous reports, we have shown that 2,6-diacetylpyridine-based Schiff-base ligands that contain rigid N_3O_2-pentadentate chelating environments can be employed to render hepta-coordinate Ln(III) complexes a pseudo-pentagonal bipyramid coordination geometry.[51,52] Moreover, the apical ligands could be made kinetically labile, and thus, such complexes could be employed further as potential magnetic building blocks for the rational syntheses of multinuclear systems in conjunction with ancillary spin connectors—especially toward the rational syntheses of single-chain magnets. In addition, these mononuclear complexes are air-stable and resistant to most of the common organic solvents, making these complexes highly potential synthons. However, such magnetic building blocks are prone to encounter octacoordination around Ln centers upon self-association with common bridging ligands owing to the strong tendency of Ln ions toward octacoordination.[33] Therefore, we intended to investigate the single-ion magnet behavior of Ln(III) ions in such octacoordinate ligand environments. Investigation of magneto−structural correlations in mononuclear systems is more preferable over polynuclear systems to minimize overparameterization.

In this regard, we have employed the 2,6-diacetylpyridine-based Schiff-base ligand containing rigid N_3O_2-pentadentate chelating environments as the basis ligand and triphenylphosphine oxide as the ancillary ligand in conjunction with Ln(III) salts to achieve a series of mononuclear octacoordinate Ln(III) complexes, [(L)Ln(TPPO)$_3$]OTf (Ln = Y (**1·Y**); Gd (**1·Gd**); Tb (**1·Tb**); Dy (**1·Dy**); Ho (**1·Ho**); and Er (**1·Er**)) and [(L)Ln(TPPO)(NO$_3$)] (Ln = Y (**2·Y**) and Dy (**2·Dy**)), where H_2L = 2,6-diacetylpyridine bis-benzoylhydrazone, TPPO = triphenylphosphine oxide, and OTf^- = trifluoromethanesulfonate. We intended to investigate how the structural and magnetic property change with the change in counter anions in the Ln salts from OTf^- to NO_3^-, keeping the basis and ancillary ligands fixed. We obtained octacoordinate mononuclear complexes for all the changes—albeit with structural variations. Magnetic property investigation was carried out on the polycrystalline solid samples of **1·Ln** (Ln = Gd, Tb, Dy, Ho, and Er) and **2·Dy**. The comparative magnetization dynamics study revealed that among all of them, **1·Dy** exhibits the highest effective energy barrier for magnetization reversal, U_{eff}/k_B = 47 K under H_{dc} = 1 kOe.

RESULTS AND DISCUSSION

Syntheses and Spectroscopic Characterization. Synthetic manipulations and sample processing for all the characterizations were carried out under aerobic conditions for all the complexes. All the complexes were synthesized upon refluxing the ligand (H_2L) with the corresponding Ln(III) salts (Ln(OTf)$_3$.*x*H$_2$O for **1·Ln** and Ln(NO$_3$)$_3$.6H$_2$O for **2·Ln**) in a 1:1 molar ratio under vigorous stirring conditions in ethanol medium, followed by treatment with triethylamine (two equivalents) as a base and triphenylphosphine oxide (six equivalents for **1·Ln** and two equivalents for **2·Ln**) at room temperature (Scheme 1, see the Experimental Section for details). The whole reaction mixture started to turn yellow with concomitant consumption of the white suspended particles of H_2L upon addition of the respective Ln(III) salt solution into the white slurry of H_2L, implying complexation of the ligand with the metal ions. Solid TPPO was added into the reaction mixture in a portion at room temperature under stirring conditions after completion of dropwise addition of two equivalents of ethanolic solution (10:1 v/v EtOH/Et$_3$N) of Et$_3$N as the base. An immediate change in the color of the whole reaction mixtures from yellow to orange-yellow was observed upon the addition of the base. The change in color could be attributed to the deprotonation of the amide protons of the ligands upon the addition of the base. The reaction mixtures were concentrated under reduced pressure after stirring at room temperature for six hours. The precipitates were isolated by filtration and recrystallized from chloroform solutions via slow evaporation to obtain the products as the polycrystalline yellow solids with excellent isolated yields (90−95%).

https://doi.org/10.1021/acsomega.2c03631
ACS Omega 2022, 7, 25881−25890

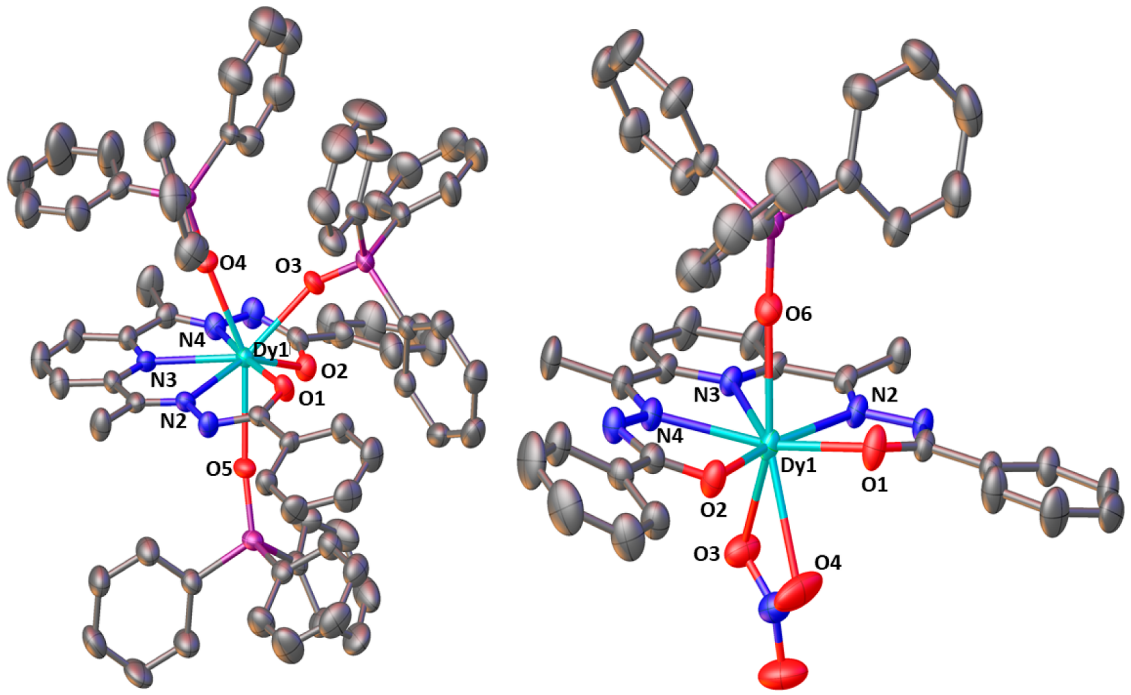

Figure 1. Ellipsoid models with 60% probability for the single-crystal X-ray molecular structures of **1·Dy** (left) and **2·Dy** (right) in the solid state. The coordinated atoms are labeled. H atoms in all the complexes and trifluoromethanesulfonate counter anions and the lower occupancy C atoms of the phenyl rings that are split due to thermal disorder in **1·Dy** are omitted for clarity. Color codes: cyan, Dy; purple, P; red, O; blue, N; and gray, C.

Table 1. Selected Crystallographic Data and Refinement Parameters for 1·Ln (Ln = Tb, Dy, Ho, and Er) and 2·Dy

	1·Tb	1·Dy	1·Ho	1·Er	2·Dy
formula[a]	C78H64F3N5O8P3STb	C78H64F3N5O8P3SDy	C78H64F3N5O8P3SHo	C78H64F3N5O8P3SEr	C41H34N6O6PDy
Mr (g mol^{-1})[a]	1540.25	1543.82	1546.25	1548.58	900.21
crystal system	*triclinic*	*triclinic*	*triclinic*	*triclinic*	*monoclinic*
space group	$P\bar{1}$	$P\bar{1}$	$P\bar{1}$	$P\bar{1}$	$P2_1/c$
T (K)	150	150	150	150	150
a (Å)	11.9500(8)	11.9315(11)	11.919(3)	11.7997(3)	13.763(3)
b (Å)	16.3190(14)	16.2476(15)	16.223(6)	16.0762(4)	9.4067(16)
c (Å)	19.3869(18)	19.3801(19)	19.402(8)	19.1850(5)	29.275(5)
α (°)	88.012(5)	88.053(5)	88.051(11)	88.274(1)	90
β (°)	75.012(5)	74.868(5)	74.865(10)	75.455(1)	97.373(9)
γ (°)	86.910(5)	87.069(5)	87.188(10)	87.074(1)	90
V (Å^3)	3645.9(5)	3621.2(6)	3616(2)	3517.49(16)	3758.7(12)
Z	2	2	2	2	4
ρcalcd. (g cm^{-3})	1.403	1.416	1.420	1.462	1.591
μ (mm^{-1})	1.131	1.194	1.256	1.360	2.087
collected reflns	10592	12536	10531	18933	14625
unique reflns	10454	12322	10032	18868	14503
no. of parameters	1005	984	999	957	496
refinement reflections.	10592	12536	10531	18933	14625
R [$I > 3\sigma(I)$][b]	0.0705	0.0492	0.0568	0.0257	0.0495
wR [$I > 3\sigma(I)$][c]	0.1565	0.1309	0.0835	0.0624	0.1246
GOF on F	0.941	1.032	0.984	1.064	1.003

[a]Excluding co-crystallized solvent molecules. [b]$R = \Sigma||F_o|-|F_c||/\Sigma|F_o|$. [c]$wR = [\Sigma(w(F_o^2-F_c^2)^2)/\Sigma([w(F_o^2)^2]^{1/2}$, where $w = 1/(\sigma^2(F_o^2) + (aP)^2 + bP)$ with $P = (2F_c^2 + \max(F_o^2,0))/3$.

A sharp change from white slurry to a yellow solution during the reactions indicated the complexation of the ligands with the metal ions. The absorbance in the visible range with the λ_{max} nearly 400 nm results in the exhibition of the characteristic yellow color of the complexes (Figure S1, see the Supporting Information). Infrared (IR) spectroscopy studies displayed a significant decrease in carbonyl stretching frequencies and an increase in imine stretching frequencies in the complexes compared to the free Schiff-base ligands (Table S1 and Figures S2 and S3). Increment of the imine stretching frequencies directly implies coordination of the ligands through imine nitrogen centers. However, electronic resonance between the

https://doi.org/10.1021/acsomega.2c03631
ACS Omega 2022, 7, 25881−25890

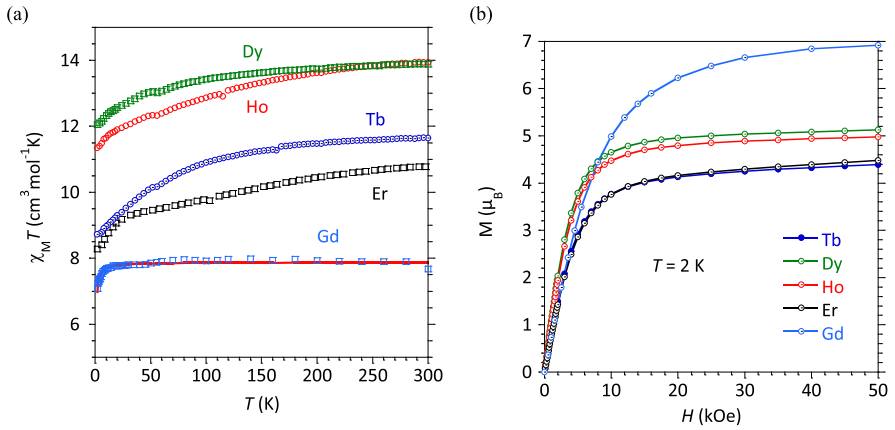

Figure 2. Magnetic behaviors for **1·Ln**: *(a)* $\chi_M T$ vs T plots and (b) M vs H for Ln = Gd, light-blue; Tb, dark blue; Dy, green; Ho, red; and Er, black. The best fit of $\chi_M T$ vs T plot for **1·Gd** is shown as the solid red line and the best-fit parameters are provided in the text. Additional plots for each derivative and for **2·D**y can be found in the Supporting Information.

amide nitrogen and the carbonyl group is expected to enhance in the deprotonated form of the ligands and thereby decreasing the bond order of the carbonyl group significantly. Consequently, the carbonyl stretching frequencies are expected to decrease in spite of the coordination through the carbonyl oxygen.

The room-temperature solution ^{1}H NMR spectroscopy studies on the Y analogues of the complexes (Figure S4) confirmed the deprotonation of the amide protons of the ligands in the complexes. Moreover, the relative integration ratios of the ^{1}H NMR signals indicated the TPPO and the Schiff-base ligand ratios to be 3:1 for **1·Ln** and 1:1 for **2·Ln**. The ^{31}P NMR spectra of the Y analogues of the complexes (Figures S5−S6) displayed downfield chemical shifts (δ = 32.14 ppm, broad, for **1·Y** in $CDCl_3$ and δ = 32.80 ppm, sharp, for **2·Y** in CD_3OD) compared to the free TPPO ligand (δ = 30.31 ppm in $CDCl_3$ and δ = 32.39 ppm in CD_3OD), thereby indicating the coordination of TPPO to the metal centers. The appearance of one signal for each of the complexes indicates the presence of a single product in the solution. However, a relatively broad ^{31}P signal for **1·Y** compared to **2·Y** could be ascribed to the presence of three magnetically different P centers in the former and one type of P center in the latter. ^{19}F (Figure S7) and ^{13}C (Figure S8) NMR spectral analyses on the Y analogues in solutions also indicated the purity of the complexes in bulk. Elemental analyses (see the Experimental Section) on the polycrystalline solid samples of the complexes revealed the chemical compositions as described in Scheme 1. Single-crystal X-ray diffraction analyses unambiguously confirmed the formation of the molecular complexes.

X-ray Crystallographic Characterization. Single-crystal X-ray diffraction analyses unequivocally revealed the structures of complexes where one molecule of the pentadentate ligand chelates an Ln(III) center through the N_3O_2 ligating environment and the meridional three coordinating sites are occupied by the ancillary ligands (three TPPO molecules for **1·Ln** and a TPPO molecule and an κ^2-NO_3^- anion for **2·Ln**) completing the octacoordination, as depicted in Scheme 1. The solid-state molecular structures are portrayed in Figure 1 for the Dy analogues as the representative structures for the respective series (**1·Dy** for **1·Ln** and **2·Dy** for **2·Ln**), while the molecular structures for the rest of the complexes are displayed in the Supporting Information (Figures S9−S16). Suitable single crystals for X-ray diffraction for the complexes were grown upon slow evaporation of the chloroform solutions of the complexes under ambient conditions.

All the complexes of the series **1·Ln** crystallize in a triclinic crystal system with the $P\bar{1}$ space group incorporating two molecules per unit cell (Figure S17). On the other hand, all the complexes of the series **2·Ln** crystallize in a monoclinic crystal system with the $P2_1/n$ space group for **2·Y** and the $P2_1/c$ space group for **2·Dy** incorporating four molecules per unit cell (Figure S17). The crystallographic data and refinement parameters for the complexes are provided in Tables 1 and S2. The selected bond lengths and bond angles associated with the coordination environments of the complexes are summarized in Table S3. As all the Ln complexes for a particular series (either **1·Ln** or **2·Ln**) are isostructural, the solid-state molecular structures are described herein only for the Dy analogues as the representative structures for their respective series.

The coordination geometries around the Ln centers of the complexes are found to be significantly distorted from the regular polyhedra expected from octacoordination. However, continuous shape measures (CShMs) analyses employing the SHAPE program[53,54] based on the Pinsky−Avnir algorithm,[55] the definitions of minimal distortion paths,[56] and generalized interconversion coordinates[57] revealed that the closest resemblance of the coordination polyhedra for all the complexes is the biaugmented trigonal prism with a C_{2v} symmetry (Table S4).

A doubly deprotonated form of the ligand chelates the Dy ion through two carbonyl oxygen (O1 and O2), two imine nitrogen (N2 and N4), and the pyridyl nitrogen (N3) atoms completing its N_3O_2 pentacoordination, leading to a pseudo-pentagonal basal plane around the Dy center, as shown in Figure 1. Interestingly, these N_3O_2 pentagonal basal planes around the Dy centers in both the series of complexes are similar to each other (Figure S18). The N_3O_2 coordinating sites of the ligand form a helical alignment around the metal center in **1·Dy**. With respect to the plane consisting of N2−N3−N4 atom sites, the Dy and O1 centers are slightly above the plane (0.189 and 0.264 Å, respectively), while the O2 center is 0.666 Å below the plane. Such a significant deviation from the planarity for O2 could be attributed to the steric hindrance caused by the phenyl groups of one of the coordinated TPPO molecules.

https://doi.org/10.1021/acsomega.2c03631
ACS Omega 2022, 7, 25881−25890

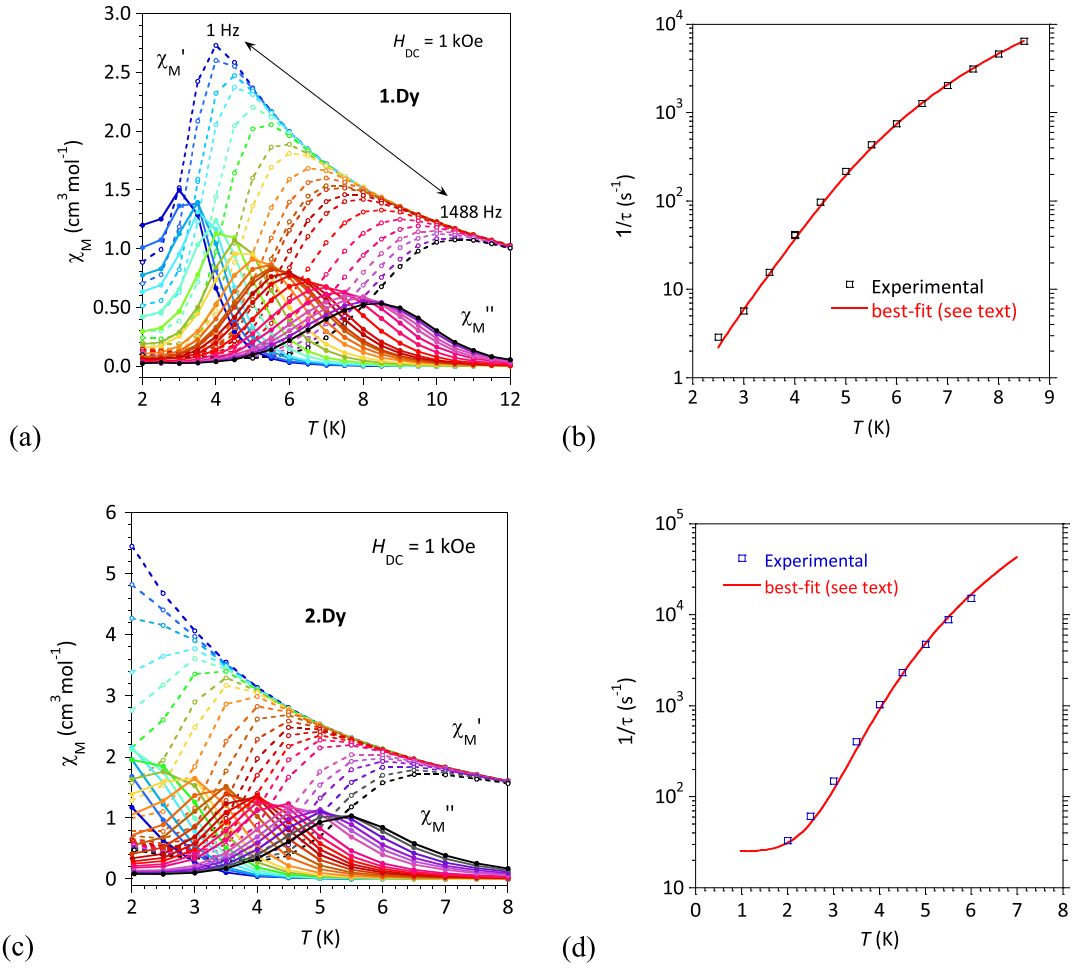

Figure 3. χ_M' and χ_M'' vs T for AC frequencies between 1 and 1488 Hz with an applied DC field of 1 kOe and a temperature dependence of the relaxation time for (a,b) **1·Dy** and (c,d) **2·Dy**.

The N_3O_2 coordination pattern in the case of **2·Dy** is similar to **1·Dy**; however, the deviation of the carbonyl oxygen atoms from the plane of pyridyl moiety (N2−N3−N4 atom sites) is significantly less for the former−the O2 and the Dy centers being above the plane (0.164 and 0.166 Å, respectively) and the O1 center being below the plane (0.327 Å). Three oxygen atoms (O3−O5) from three TPPO molecules coordinate with the Dy center of **1·Dy** in such a fashion that they (O3−O5 and Dy) constitute a near-meridional plane (O3−Dy−O4−O5 dihedral angle 8.6^0) with respect to the N_3O_2 basal plane and thus completing the octacoordination around the Dy center (Figure 1, left). However, two oxygen atoms (O3−O4) of a chelating κ^2-NO_3^- anion, an oxygen atom (O6) of a coordinated TPPO molecule, and the Dy center constitute such a meridional plane (O3−Dy−O4−O6 dihedral angle 11.5^0) for **2·Dy** (Figure 1, right). The solid-state packing diagrams for **1·Dy** displayed two molecular complexes per unit cell where the molecules are aligned along the longest cell length with a Dy−Dy distance of 13.03 Å (Figure S17). Therefore, the distance between two nearest-neighboring Dy−Dy centers in the three-dimensional packing corresponds to the smallest cell length, that is, 11.93 Å. On the other hand, there are four molecules per unit cell for **2·Dy** where the distance between two nearest-neighboring Dy−Dy centers is 7.57 Å (Figure S17). The solid-state phase purity for all the complexes was confirmed by powder X-ray diffraction (PXRD) analyses on the polycrystalline solid samples of all the complexes. The comparative experimental and simulated PXRD patterns for all the complexes are displayed in the Supporting Information (Figures S19). An excellent agreement between the experimental PXRD patterns and the simulated PXRD patterns revealed the phase purity of the isolated products.

Magnetic Property Investigation. The temperature dependence of the molar magnetic susceptibilities, χ_M, for all the complexes were investigated over the temperature range of 2−300 K, and the results are plotted as $\chi_M T$ versus T in Figure 2 for **1·Ln** (Ln = Gd, Tb, Dy, Ho, and Er) and in Figure S25 for **2·Dy**. The experimentally observed $\chi_M T$ values (in cm^{3}mol^{-1}K^{-1} unit) at 300 K are found to be 7.83 (**1·Gd**), 11.65 (**1·Tb**), 13.9 (**1·Dy**), 13.93 (**1·Ho**), 10.80 (**1·Er**), and 14.15 (**2·Dy**). Each of these values agrees well with the theoretical value considering the magnetically exchange-free single Ln^{III} ion (7.88 for Gd^{III} ion with S = 7/2, g_{iso} = 2; 11.82 for Tb^{III} ion with J = 6, g_J = 3/2; 14.17 for Dy^{III} ion with J = 15/2, g_J = 4/3; 14.07 for Ho^{III} with J = 8, g_J = 5/4; and 11.48 for Er^{III} with J = 15/2, g_J = 6/5). Upon lowering the temperature, the $\chi_M T$ values gradually decreased to 8.7 (**1·Tb**), 12.0 (**1·Dy**), 11.3 (**1·Ho**), 19.3 (**1·Er**), and 12.9 (**2·Dy**) at 2 K (Figure 2). Such a decrease in the $\chi_M T$ value is expected for these ions due to the CF effects and the subsequent depopulation of the magnetic states upon lowering the

https://doi.org/10.1021/acsomega.2c03631
ACS Omega 2022, 7, 25881−25890

temperature. On the other hand, the $\chi_M T$ values for **1·Gd** remained almost unchanged up to around 10 K before a slight decrease upon further lowering the temperature. The concomitant fitting of the temperature-dependent magnetic susceptibility and variable temperature field-dependent magnetization resulted the best-fit parameters g-factor, g_{iso} = 1.999, ZFS parameter, D = 0.283 cm^{-1}, and mean field intermolecular magnetic interactions, z_J' = −0.007 cm^{-1}—confirming isolated magnetic centers in the solid state (Figures 2a and S20).

The field dependence of the magnetizations was studied in the field range of 0−5 T at the temperatures of 2, 3, 5, and 7 K and plotted as M versus H (Figures 2b and S21−25), except for **1·Gd**, which is investigated in the field range of 0−7 T at 1.8, 5, and 8 K (Figure S20). The molar magnetizations (in μ_B unit) of the complexes at 2 K and 5 T (at 1.8 K and 7 T for **1·Gd**) are found to be 7.0 (**1·Gd**), 4.4 (**1·Tb**), 5.1 (**1·Dy**), 5.0 (**1·Ho**), 4.5 (**1·Er**), and 5.4 (**2·Dy**), which are well within the range of the generally observed values for the mononuclear complexes of these Ln^{III} ions.

In order to have an insight into the magnetization blocking and slow relaxation of the magnetization, AC susceptibility has been investigated for all the complexes (except Gd and Y analogues) both in the absence of and under the applied DC magnetic fields (Figures S21−25). No or just the onset of an *out-of-phase* AC susceptibility (χ'') component was found above 2 K except for **1·Dy** and **2·Dy**, for which well-defined blocking temperatures were detected at approximately 9 and 6 K, respectively, at an AC frequency of 1.5 kHz under the applied DC field of 1 kOe (Figures S22 and S25). Therefore, detailed variable temperature variable frequency AC magnetic susceptibilities were investigated under an applied DC field of 1 kOe only for **1·Dy** and **2·Dy**. The resulting frequency and temperature dependences are plotted in Figures 3, S22, and S25.

$$\tau^{-1} = \tau_0^{-1} e^{-U_{eff}/k_B T} + AT^n + \tau_{QTM}^{-1} \quad (1)$$

The temperature and frequency dependences of the maxima exhibited by the χ_M'' versus T and χ_M'' versus ν behaviors revealed slow magnetic relaxation for both **1·Dy** and **2·Dy**. The relaxation times, τ, were deduced from χ_M'' as a function of frequency using the generalized Debye model, and they are plotted against temperature in Figure 3. Analysis of the relaxation time distribution width indicated very small values for the α-parameters with, however, a slight increase for the lower temperature domain (see Figures S22 and S25). This implied a dominant single relaxation process in the higher T range and an additional relaxation contribution for the lower T. Best modeling of the temperature dependence of the relaxation time for **1·Dy** was obtained by considering a relaxation driven by Orbach−Raman mechanisms (respectively the first and second terms in eq 1). However, for **2·Dy**, an additional contribution from QTM (quantum tunneling of the magnetization, third term in eq 1) had to be added to well reproduce the lower temperature behavior (Figure 3). The best-fit parameters are for **1·Dy** U_{eff}/k_B = 47 K, $\tau_0 = 8 \times 10^{-7}$ s, A = 0.01 $s^{-1}K^{-n}$, and n = 5, and for **2·Dy** U_{eff}/k_B = 39 K, $\tau_0 = 1 \times 10^{-7}$ s, A = 0.07 $s^{-1}K^{-n}$, n = 6, and τ_{QTM} = 0.04 s. Both the complexes exhibit an energy barrier for magnetization reversal (U_{eff}/k_B), which reflects the very close coordination sphere for Dy(III) in **1·Dy** and **2·Dy**.

Evidently, the Dy(III) ion with a similar N_3O_2-pentadentate basal plane but in a pentagonal bipyramidal coordination geometry, where an oxygen of phosphine oxide and a chloride ion are at the axial coordination sites ([(L)Dy(OPR_3)Cl], R = alkyl/aryl substituents), inherits the magnetic ground states that are very close (>95%) to the pristine eigenstates of $M_J = \pm 15/2$.[52] These complexes exhibit field-induced slow relaxation of magnetization dominantly via the Orbach mechanism with effective energy barriers in the range of 204−241 K. Moreover, the magnetic anisotropy axis lies on the N_3O_2-pentadentate basal plane and is oriented along the line that is almost perpendicular to the Dy−N(pyridine) bond, which implies that the keto-imine bonds exert strong enough CF strength to dictate the orientation of the magnetic anisotropy axis in this series of complexes. However, for the homoleptic octacoordinate Dy(III) complexes with higher CF symmetry (cubic, square-prism/antiprism, and hexagonal bipyramid), the ground magnetic eigenstates are dominantly characterized with $M_J = \pm 15/2$, and the magnetic anisotropy axis operates along the principal symmetry axis of the inner coordination sphere.[26] On the other hand, for the lower symmetry octacoordinate Dy(III) complexes, the ground magnetic eigenstates are still mostly characterized with $M_J = \pm 15/2$, while the orientation of the magnetic anisotropy axis is subject to the distribution of the CF strength in the inner coordination sphere.[58] The coordination symmetries of the complexes described herein can be assigned to a distorted biaugmented trigonal prism J50 (C_{2v}) (BTPR) (Table S4), and obviously, they can be categorized as less symmetric, even notwithstanding the heteroleptic coordination environments. Among the series of lower symmetric octacoordinate Dy(III) complexes analyzed by Chilton, N. F. et al.,[58] the coordination geometries of [Dy(phen)$(acac)_3$][59] and [Dy(paaH*)$_2(H_2O)_4$]$(Cl)_3$[59] could be regarded as the closest to those of **1·Dy** and **2·Dy**, respectively. However, the degrees of distortions from the regular polyhedra are more for **1·Dy** and **2·Dy** than [Dy(phen)$(acac)_3$] and [Dy(paaH*)$_2(H_2O)_4$]$(Cl)_3$ (Table S4). The closest two regular polyhedra that resemble to the coordination geometry in both **1·Dy** and [Dy(phen)$(acac)_3$] are square antiprism (D_{4d}) (SAPR) and BTPR with the *SHAPE analysis* minimal distortion path values 5.156 and 5.037, respectively, for **1·Dy** and 0.425 and 2.473, respectively, for [Dy(phen)$(acac)_3$] (Table S4). On the other hand, the closest two regular polyhedra that resemble to the coordination geometry in both **2·Dy** and [Dy(paaH*)$_2(H_2O)_4$]$(Cl)_3$ are triangular dodecahedron (D_{2d}) (TDD) and BTPR with the *SHAPE analysis* minimal distortion path values 4.071 and 3.575, respectively, for **2·Dy** and 0.338 and 1.944, respectively, for [Dy(paaH*)$_2(H_2O)_4$]$(Cl)_3$ (Table S4). Both [Dy(phen)-$(acac)_3$][59] and [Dy(paaH*)$_2(H_2O)_4$]$(Cl)_3$[60] exhibit zero-field slow relaxation of magnetization dominantly via the Orbach mechanism with effective energy barriers, U_{eff} = 64 and 179 K, respectively. Despite higher coordination symmetry in the former (D_{4d}) than the latter (D_{2d}), higher U_{eff} value for the later could be ascribed to two main factors—the (tri)cationic nature rendering a stronger CF and a homoleptic coordination environment resulting in uniform CF distribution and thereby reducing the QTM. Lower U_{eff} values for **1·Dy** and **2·Dy** especially compared to [Dy(paaH*)$_2(H_2O)_4$]$(Cl)_3$ could be attributed to lesser ionic charge, higher degrees of geometric distortions, and heteroleptic coordination environments in the formers. Comparatively, the symmetry of the regular polyhedron (BTPR) that is closest to the coordination geometries in both **1·Dy** and **2·Dy** is the same (C_{2v}), although the deviation from the BTPR is more for the former. However,

https://doi.org/10.1021/acsomega.2c03631
ACS Omega 2022, 7, 25881−25890

1·Dy is cationic in nature, while **2·Dy** is a neutral complex. In addition, one of the coordinated TPPO molecules which is inclined toward the equatorial plane in **1·Dy** renders significant steric hindrance with the pentadentate chelating ligand. Such an impact is absent in **2·Dy**. This is evidenced from the larger average Ln-equatorial bond distances in **1·Dy** (Dy1-O1: 2.301, Dy1-O2: 2.365, Dy1-N4: 2.512, Dy1-N2: 2.523, and Dy1-N3: 2.570; Figure 1) than **2·Dy** (Dy1-O1: 2.280, Dy1-O2: 2.252, Dy1-N4: 2.431, Dy1-N3: 2.432, and Dy1-N2: 2.439). At the same time, the average Ln-axial bond distances are shorter in **1·Dy** (Dy1-O4: 2.306, Dy1-O5: 2.308, and Dy1-O3: 2.363) than **2·Dy** (Dy1-O6: 2.288, Dy1-O4: 2.442, and Dy1-O3: 2.466). Therefore, the CF strength is more uniformly distributed in **1·Dy** than **2·Dy**. Consequently, less QTM and higher U_{eff} are expected for **1·Dy** than **2·Dy**, which is reflected from their AC magnetic susceptibilities as described above. Significantly lower U_{eff} values of **1·Dy** (or **2·Dy**) than ([(L)Dy(OPR_3)Cl] could originate from the additional coordination bond that lifts the symmetry and thereby enhances QTM in the former. It is worth mentioning that the Dy(III) ion with such an N_3O_2-pentacoordinate base shows a better *Ising-type* magnetic building block when the coordination geometry has higher symmetry, such as a pentagonal bipyramid.[51,52] However, octacoordinate Dy(III) building blocks accompanied with such an N_3O_2-pentacoordinate base can be regarded to have more potential considering the stronger affinity of Ln(III) ions to adopt octacoordination, and they encompass wider varieties of bridging ligands as spin connectors.[33]

CONCLUSIONS

In conclusion, we have employed the N_3O_3-pentadentate rigid Schiff base as the basis ligand in conjunction with triphenylphosphine oxide/nitrate as the ancillary ligands to investigate structural variation around eight-coordinated trivalent lanthanide ions. For all these complexes, the coordination spheres comprise a doubly deprotonated N_3O_2-pentadentate ligand forming an approximate pentagonal basal plane and three O-atoms. The latter are provided either by one TPPO and a κ^2-NO_3^- anion (**2·Ln**) or by three $OPPh_3$ molecules (**1·Ln**), leading to a different CF environment. This geometrical consideration translates to the characteristics of the slow relaxation of the magnetization exhibited by the Dy analogues. The higher blocking temperature for **1·Dy** compared to **2·Dy** (respectively 47 and 39 K) is attributed to mainly the cationic nature and the higher CF symmetry in the former. The Dy(III) complexes with such N_3O_2-pentacoordinate base could be employed as the potential magnetic building blocks for the syntheses of polynuclear single-molecule and single-chain magnets. The potential advantages of such magnetic building blocks include the SIM behavior even in lower symmetry coordination, the stability in most of the common organic solvents, and the capability of being post-synthetically modified in an inner coordination sphere.

EXPERIMENTAL SECTION

Materials and Methods. All the reagents and solvents used for the syntheses were used as received from the commercial suppliers. The Schiff-base ligand H_2L was synthesized following the reported procedure.[61] TPPO was synthesized starting from triphenylphosphine following the reported procedure.[62] Syntheses and manipulations of samples for all the experiments were carried out under aerobic conditions. All the spectroscopy studies were carried out at ambient conditions. UV−vis spectral studies were carried out on μ(M) ethanol solutions of the complexes using an Agilent Hewlett-Packard 8453 diode array UV−Vis spectrometer. The ^{1}H and ^{31}P NMR spectral studies were carried out for the Y analogues of the complexes in deuterated solvents (CDCl3 for **1·Y** and CD3OD for **2·Y**) chloroform with a Bruker model Ascend 400 FT-NMR spectrometer. Fourier transform infrared (FT-IR) spectroscopy studies were performed on the thin layers of neat samples with a Bruker-Alpha Eco-ATR FT-IR spectrometer. Elemental analyses were performed on the polycrystalline solid samples of the complexes with a Perkin−Elmer 2400 series II instrument.

X-ray Crystallographic Studies. Suitable single crystals for X-ray diffraction were coated with paratone oil and mounted onto a goniometer. The X-ray crystallographic data were obtained from either a Rigaku or a Bruker (D8 Advance, Da Vinci) diffractometer using the MoK_α radiation source and equipped with an Oxford Cryosystem. The structures have been solved by direct methods using SIR92 or Superflip and refined by means of least-squares procedures on F using the PC version of the program Olex2. The scattering factors for all the atoms were used as listed in the International Tables for X-ray Crystallography.[63] Absorption correction was performed using a multiscan procedure. The H atoms were repositioned geometrically. The H atoms were initially refined with soft restraints on the bond lengths and angles to regularize their geometry and $U \sim$ iso~(H) (in the range 1.2−1.5 times $U \sim$ eq~ of the parent atom), after which the positions were refined with riding constraints. All non-hydrogen atoms were refined anisotropically. The crystallographic data and refinement parameters for the single-crystal X-ray data analyses for the complexes **1·Ln** are summarized in Table 1, while that for the rest of the complexes given in the Supporting Information (Table S1). The selected bond parameters are provided in the Supporting Information (Tables S2). CIF data have been deposited at CCDC (http://www.ccdc.cam.ac.uk) with references 2160196−2160203 for the complexes **1·Y**, **1·Tb**, **1·Dy**, **1·Ho**, **1·Er**, **2·Y**, and **2·Dy**. The solid-state phase purity of the isolated polycrystalline solid samples of the complexes was confirmed by powder X-ray diffraction (PXRD) using a Rigaku (SmartLab) diffractometer with the Cu(Kα) radiation source radiation, λ = 1.5406 Å. The PXRD studies were carried out with 2θ ranging from 5 to 50° with a step size of 0.01.

Magnetic Property Measurements. Magnetic measurements for all the samples were carried out with a Quantum Design MPMS 5S SQUID magnetometer in the temperature range of 2−300 K. The measurements were performed on polycrystalline samples. The freshly isolated crystalline powders of the complexes were mixed with grease (except for Gd complex) and put in gelatin capsules. The temperature dependences of the magnetization were measured in an applied field of 1 kOe, and the isothermal field dependence of the magnetizations were collected up to 5 or 7 T. The molar susceptibility (χ_M) was corrected for sample holder, grease, and for the diamagnetic contribution of all the atoms by using Pascal's tables.[64] The magnetic data for **1-Gd** were fitted using the spin Hamiltonians as coded in the PHI software.[65] AC susceptibility has been collected using an AC field of 3 Oe over a frequency range of 1−1500 Hz in a zero field and with applied fields.

https://doi.org/10.1021/acsomega.2c03631
ACS Omega 2022, 7, 25881−25890

SYNTHETIC PROCEDURES

General Synthetic Procedure. A 100 mL two-necked round-bottom flask was equipped with a magnetic stirring bar and 0.2 mmol of a lanthanide salt (139.6 mg for $Y(OTf)_3 \cdot 9H_2O$; 121 mg for $Gd(OTf)_3$; 153.9 mg for $Tb(OTf)_3 \cdot 9H_2O$; 154.4 mg for $Dy(OTf)_3 \cdot 9H_2O$; 154.9 mg for $Ho(OTf)_3 \cdot 9H_2O$; 155.3 mg for $Er(OTf)_3 \cdot 9H_2O$; 73.1 mg for $Y(NO_3)_3 \cdot 5H_2O$; and 87.7 mg for $Dy(NO_3)_3 \cdot 5H_2O$). The lanthanide solid was dissolved in a minimum amount of absolute ethanol under stirring at room temperature before setting it up on an oil bath at 50−60 °C. A slurry of 0.2 mmol of the ligand (79.8 mg for H_2L) was suspended in 45−50 mL of absolute ethanol and was then slowly added into the solution of the lanthanide salt under vigorous stirring condition at 50−60 °C in a time period of 5−6 min. After completion of the addition of the ligand slurry into the salt solution, the reaction mixture was set to reflux under stirring conditions for 1 h, followed by cooling down the reaction mixture to room temperature to obtain a transparent yellow solution. A solid of TPPO was added in a portion to the reaction mixture under stirring condition at room temperature. Once all the solid particles of TPPO got dissolved, 0.4 mmol of Et_3N (40.5 mg) was added, and the reaction mixture was kept under stirring for 6 h at room temperature. A yellow precipitate appeared in due course. The reaction mixture was concentrated to 20−25 mL under reduced pressure, followed by filtering off the solid which was recrystallized from the saturated solution in chloroform via slow evaporation under ambient conditions to obtain the product as a polycrystalline yellow solid. Good-quality single crystals suitable for X-ray diffraction were grown by slow evaporation of the chloroform solution under a desiccator.

*[(L)Y(TPPO)$_3$]OTf (**1·Y**).* Isolated yield 90% (265 mg). UV−vis: λ_{max} = 344 nm; ε = 2.28 × 10^4 $Lmol^{-1}cm^{-1}$. NMR ($CDCl_3$): δ ppm: ^{1}H: 2.33 (s, 6H,−CH_3) 7.27−7.30 (b,12H, Aromatic −CH) 7.35−7.49 (m, 44H, Aromatic −CH) 8.04−8.18 (b,2H, Aromatic −CH). ^{13}C: 8.87, 46.98, 128.06, 128.64, 128.77, 128.97, 130.10, 131.15, 131.89, 131.99, 132.48, 132.50. ^{19}F: −78.20. ^{31}P: 32.13. IR (cm^{-1}): $\upsilon_{C=O}$ = 1556 (s) and 1589(s); $\upsilon_{C=N}$ = 1551(m). Elemental analysis (%) calcd for $C_{78}H_{64}F_3N_5O_8P_3SY$ (FW = 1470.28 g/mol): C 63.72; H 4.39; N 4.76; found, C 63.64; H 4.40; N 4.74.

[(L)Gd(TPPO)$_3$]OTf (1·Gd). Isolated yield 93% (285 mg). UV−vis: λ_{max} = 344 nm; ε = 2.28 × 10^4 $Lmol^{-1}cm^{-1}$. IR (cm^{-1}): $\upsilon_{C=O}$ = 1555 (s) and 1589(s); $\upsilon_{C=N}$ = 1551(m). Elemental analysis (%) calcd for $C_{78}H_{64}F_3N_5O_8P_3SGd$ (FW = 1538.62 g/mol): C 60.89; H 4.19; N 4.76; found, C 60.74; H 4.21; N 4.73.

[(L)Tb(TPPO)$_3$]OTf (1·Tb). Isolated yield 85% (261 mg). UV−vis: λ_{max} = 345 nm; ε = 2.72 × 10^4 $Lmol^{-1}cm^{-1}$. IR (cm^{-1}): $\upsilon_{C=O}$ = 1556(m); $\upsilon_{C=N}$ = 1633 (b) and 1588 (s). Elemental analysis (%) calcd for $C_{78}H_{64}F_3N_5O_8P_3SDy$ (FW = 1540.30 g/mol): C 60.82; H 4.19; N 4.55; found, C 60.74; H 4.20; N 4.54.

[(L)Dy(TPPO)$_3$]OTf (1·Dy). Isolated yield 85% (262 mg). UV−vis: λ_{max} = 342 nm; ε = 4.71 × 10^4 $Lmol^{-1}cm^{-1}$. IR (cm^{-1}): $\upsilon_{C=O}$ = 1556(m) and 1539(m); $\upsilon_{C=N}$ = 1630(m) and 1587 (m). Elemental analysis (%) calcd for $C_{78}H_{64}F_3N_5O_8P_3SDy$ (FW = 1543.87 g/mol)): C 60.68; H 4.18; N 4.54; found, C 60.56; H 4.20; N 4.53.

[(L)Ho(TPPO)$_3$]OTf (1·Ho). Isolated yield 89% (275 mg). UV−vis: λ_{max} = 345 nm; ε = 3.07 × 10^4 $Lmol^{-1}cm^{-1}$. IR (cm^{-1}): $\upsilon_{C=O}$ = 1556(m) and 1589(s); $\upsilon_{C=N}$ = 1635(w) and 1590 (m). Elemental analysis (%) calcd for $C_{78}H_{64}F_3N_5O_8P_3SHo$ (FW = 1546.30 g/mol): C 60.59; H 4.17; N 4.53; found, C 60.57; H 4.18; N 4.51.

[(L)Er(TPPO)$_3$]OTf (1·Er). Isolated yield 85% (263 mg). UV−vis: λ_{max} = 340 nm; ε = 6.25 × 10^4 $Lmol^{-1}cm^{-1}$. IR (cm^{-1}): $\upsilon_{C=O}$ = 1555(m) and 1541(m); $\upsilon_{C=N}$ = 1632(m) and 1588 (m). Elemental analysis (%) calcd. for $C_{78}H_{64}F_3N_5O_8P_3SEr$ (FW = 1548.63 g/mol): C 60.50; H 4.17; N 4.52; found, C 60.44; H 4.18; N 4.50.

[(L)Y(TPPO) (NO$_3$)] (2·Y). Isolated yield 86% (142 mg). UV−vis: λ_{max} = 344 nm; ε = 4.93 × 10^4 $Lmol^{-1}cm^{-1}$. NMR(CD_3OD): δ ppm: ^{1}H: 2.68 (s, 6H, −CH3) 7.44−7.67 (m, 21H, Aromatic −CH) 7.94−7.97 (d,2H, Aromatic −CH) 8.20−8.33 (m,5H, Aromatic −CH). ^{13}C: 12.10,122.51, 127.55, 128.51, 128.58, 128.63,130.50, 131.63, 131.74, 132.41, 132.44,135.46, 141.47, 154.90, 155.12, 175.23. ^{31}P: 32.79. IR (cm^{-1}): $\upsilon_{C=O}$ = 1554(m); $\upsilon_{C=N}$ = 1587(m). Elemental analysis (%) calcd. for $C_{41}H_{34}N_6O_6PY$ (FW = 826.64 g/mol): C 59.57; H 4.15; N 10.17; found, C 59.44; H 4.17; N 10.14.

[(L)Dy(TPPO) (NO$_3$)] (2·Dy). Isolated yield 88% (158 mg). UV−vis: λ_{max} = 345 nm; ε = 5.99 × 10^4 $Lmol^{-1}cm^{-1}$. IR (cm^{-1}): $\upsilon_{C=O}$ = 1555(m); $\upsilon_{C=N}$ = 1587(m). Elemental analysis (%) calcd. for $C_{41}H_{34}N_6O_6PDy$ (FW = 900.23 g/mol): C 54.70; H 4.81; N 9.34; found, C 54.66; H 4.83; N 9.24.

ASSOCIATED CONTENT

Supporting Information

The Supporting Information is available free of charge at https://pubs.acs.org/doi/10.1021/acsomega.2c03631.

UV−vis, IR, and NMR spectra; single-crystal X-ray structures and the coordination polyhedra; powder X-ray diffractograms; crystallographic data and refinement parameters; crystallographic bond parameters; SHAPE analysis data; and additional magnetic properties analyses plots are available at https://pubs.acs.org/doi/xxxxx. The crystallographic data have been deposited at the Cambridge Crystallographic Data Center with reference number CCDC 2160196−2160203. The data can be obtained free of charge from The Cambridge Crystallographic Data Centre via http://www.ccdc.cam.ac.uk/data_request/cif (PDF)

Crystallographic data for complexes **1**−**2** (CIF)

AUTHOR INFORMATION

Corresponding Authors

Jean-Pascal Sutter − *Laboratoire de Chimie de Coordination Du CNRS (LCC-CNRS), Université de Toulouse, CNRS, Toulouse 31062, France*; Email: jean-pascal.sutter@lcc-toulouse.fr

Vadapalli Chandrasekhar − *Tata Institute of Fundamental Research Hyderabad, Hyderabad 500107, India*; orcid.org/0000-0003-1968-2980; Email: vc@tifrh.res.in, vc@iitk.ac.in

Arun Kumar Bar − *Indian Institute of Science Education and Research Tirupati, Tirupati 517507 AP, India*; orcid.org/0000-0003-1261-327X; Email: a.bar@iisertirupati.ac.in

Authors

Vaibhav Singh − *Indian Institute of Science Education and Research Tirupati, Tirupati 517507 AP, India*; orcid.org/0000-0001-7635-9122

https://doi.org/10.1021/acsomega.2c03631
ACS Omega 2022, 7, 25881−25890

Dhiraj Das − *Indian Institute of Science Education and Research Tirupati, Tirupati 517507 AP, India*
Srinivas Anga − *Tata Institute of Fundamental Research Hyderabad, Hyderabad 500107, India*

Complete contact information is available at: https://pubs.acs.org/10.1021/acsomega.2c03631

Author Contributions

The manuscript was written through contributions of all authors. All the authors have given approval to the final version of the manuscript.

Funding

Funding was provided by the Ministry of Education, Government of India, via Scheme for Transformational and Advanced Research in Sciences (STARS, MoE/STARS-1/Apr2019/333).

Notes

The authors declare no competing financial interest.

■ ACKNOWLEDGMENTS

A.K.B. thanks the Ministry of Education, Government of India, for the financial aid through the Scheme for Transformational and Advanced Research in Sciences (STARS, MoE/STARS-1/Apr2019/333).

■ REFERENCES

(1) Christou, G.; Gatteschi, D.; Hendrickson, D. N.; Sessoli, R. Single-Molecule Magnets. *MRS Bull* **2011**, *25*, 66−71.
(2) Christou, G.; Gatteschi, D.; Hendrickson, D. N.; Sessoli, R. Single-Molecule Magnets. *MRS Bull.* **2000**, *25*, 66−71.
(3) Troiani, F.; Affronte, M. Molecular spins for quantum information technologies. *Chem. Soc. Rev.* **2011**, *40*, 3119−3129.
(4) Stamp, P. C. E.; Gaita-Ariño, A. Spin-based quantum computers made by chemistry: hows and whys. *J. Mater. Chem.* **2009**, *19*, 1718−1730.
(5) Ardavan, A.; Blundell, S. J. Storing quantum information in chemically engineered nanoscale magnets. *J. Mater. Chem.* **2009**, *19*, 1754−1760.
(6) Affronte, M. Molecular nanomagnets for information technologies. *J. Mater. Chem.* **2009**, *19*, 1731−1737.
(7) Aromí, G.; Aguilà, D.; Gamez, P.; Luis, F.; Roubeau, O. Design of magnetic coordination complexes for quantum computing. *Chem. Soc. Rev.* **2012**, *41*, 537−546.
(8) Katoh, K.; Isshiki, H.; Komeda, T.; Yamashita, M. Multiple-decker phthalocyaninato Tb(III) single-molecule magnets and Y(III) complexes for next generation devices. *Coord. Chem. Rev.* **2011**, *255*, 2124−2148.
(9) Ishikawa, N.; Sugita, M.; Ishikawa, T.; Koshihara, S.-y.; Kaizu, Y. Lanthanide double-decker complexes functioning as magnets at the single-molecular level. *J. Am. Chem. Soc.* **2003**, *125*, 8694−8695.
(10) Ishikawa, N.; Sugita, M.; Ishikawa, T.; Koshihara, S.-y.; Kaizu, Y. Mononuclear Lanthanide Complexes with a Long Magnetization Relaxation Time at High Temperatures: A New Category of Magnets at the Single-Molecular Level. *J. Phys. Chem. B* **2004**, *108*, 11265−11271.
(11) Guo, F.-S.; Bar, A. K.; Layfield, R. A. Main Group Chemistry at the Interface with Molecular Magnetism. *Chem. Rev.* **2019**, *119*, 8479−8505.
(12) Woodruff, D. N.; Winpenny, R. E. P.; Layfield, R. A. Lanthanide single-molecule magnets. *Chem. Rev.* **2013**, *113*, 5110−5148.
(13) Zhang, P.; Zhang, L.; Tang, J. Lanthanide single molecule magnets: progress and perspective. *Dalton Trans.* **2015**, *44*, 3923−3929.
(14) Sorace, L.; Benelli, C.; Gatteschi, D. Lanthanides in molecular magnetism: old tools in a new field. *Chem. Soc. Rev.* **2011**, *40*, 3092−3104.
(15) Habib, F.; Murugesu, M. Lessons learned from dinuclear lanthanide nano-magnets. *Chem. Soc. Rev.* **2013**, *42*, 3278−3288.
(16) Cador, O.; Le Guennic, B.; Ouahab, L.; Pointillart, F. Decorated Tetrathiafulvalene-Based Ligands: Powerful Chemical Tools for the Design of Single-Molecule Magnets. *Eur. J. Inorg. Chem.* **2020**, *2020*, 148−164.
(17) Katoh, K.; Breedlove, B. K.; Yamashita, M. Symmetry of octa-coordination environment has a substantial influence on dinuclear TbIII triple-decker single-molecule magnets. *Chem. Sci.* **2016**, *7*, 4329−4340.
(18) Bar, A. K.; Kalita, P.; Singh, M. K.; Rajaraman, G.; Chandrasekhar, V. Low-coordinate mononuclear lanthanide complexes as molecular nanomagnets. *Coord. Chem. Rev.* **2018**, *367*, 163−216.
(19) Chakraborty, A.; Goura, J.; Kalita, P.; Swain, A.; Rajaraman, G.; Chandrasekhar, V. Heterometallic 3d−4f single molecule magnets containing diamagnetic metal ions. *Dalton Trans.* **2018**, *47*, 8841−8864.
(20) Zhang, P.; Guo, Y.-N.; Tang, J. Recent advances in dysprosium-based single molecule magnets: Structural overview and synthetic strategies. *Coord. Chem. Rev.* **2013**, *257*, 1728−1763.
(21) Guo, Y.-N.; Xu, G.-F.; Guo, Y.; Tang, J. Relaxation dynamics of dysprosium(III) single molecule magnets. *Dalton Trans.* **2011**, *40*, 9953−9963.
(22) Layfield, R. A.; Murugesu, M. *Lanthanides and Actinides in Molecular Magnetism*; Wiley VCH, 2015.
(23) Rinehart, J. D.; Long, J. R. Exploiting single-ion anisotropy in the design of f-element single-molecule magnets. *Chem. Sci.* **2011**, *2*, 2078.
(24) Meng, Y.-S.; Jiang, S.-D.; Wang, B.-W.; Gao, S. Understanding the Magnetic Anisotropy toward Single-Ion Magnets. *Acc. Chem. Res.* **2016**, *49*, 2381−2389.
(25) Harriman, K. L. M.; Murugesu, M. An Organolanthanide Building Block Approach to Single-Molecule Magnets. *Acc. Chem. Res.* **2016**, *49*, 1158−1167.
(26) Ungur, L.; Chibotaru, L. F. Strategies toward High-Temperature Lanthanide-Based Single-Molecule Magnets. *Inorg. Chem.* **2016**, *55*, 10043−10056.
(27) Day, B. M.; Guo, F.-S.; Layfield, R. A. Cyclopentadienyl Ligands in Lanthanide Single-Molecule Magnets: One Ring To Rule Them All? *Acc. Chem. Res.* **2018**, *51*, 1880−1889.
(28) Guo, F.-S.; Day, B. M.; Chen, Y.-C.; Tong, M.-L.; Mansikkamäki, A.; Layfield, R. A. Magnetic hysteresis up to 80 kelvin in a dysprosium metallocene single-molecule magnet. *Science* **2018**, *362*, 1400−1403.
(29) Goodwin, C. A. P.; Ortu, F.; Reta, D.; Chilton, N. F.; Mills, D. P. Molecular magnetic hysteresis at 60 kelvin in dysprosocenium. *Nature* **2017**, *548*, 439−442 Letter.
(30) Gould, C. A.; McClain, K. R.; Reta, D.; Kragskow, J. G. C.; Marchiori, D. A.; Lachman, E.; Choi, E.-S.; Analytis, J. G.; Britt, R. D.; Chilton, N. F.; et al. Ultrahard magnetism from mixed-valence dilanthanide complexes with metal-metal bonding. *Science* **2022**, *375*, 198−202.
(31) Randall McClain, K.; Gould, C. A.; Chakarawet, K.; Teat, S. J.; Groshens, T. J.; Long, J. R.; Harvey, B. G. High-temperature magnetic blocking and magneto-structural correlations in a series of dysprosium(iii) metallocenium single-molecule magnets. *Chem. Sci.* **2018**, *9*, 8492−8503.
(32) Huang, C.-H. *Rare Earth Coordination Chemistry: Fundamentals and Applications*; John, Wiley & Sons (Asia) Pte Ltd, 2010.
(33) Bünzli, J.-C. G. Review: Lanthanide coordination chemistry: from old concepts to coordination polymers. *J. Coord. Chem.* **2014**, *67*, 3706−3733.
(34) Guo, F.-S.; Day, B. M.; Chen, Y.-C.; Tong, M.-L.; Mansikkamäki, A.; Layfield, R. A. A Dysprosium Metallocene

Single-Molecule Magnet Functioning at the Axial Limit. *Angew. Chem., Int. Ed. Engl.* **2017**, *56*, 11445−11449.
(35) Chilton, N. F.; Goodwin, C. A. P.; Mills, D. P.; Winpenny, R. E. P. The first near-linear bis(amide) f-block complex: a blueprint for a high temperature single molecule magnet. *Chem. Commun.* **2015**, *51*, 101−103.
(36) Chilton, N. F. Design Criteria for High-Temperature Single-Molecule Magnets. *Inorg. Chem.* **2015**, *54*, 2097−2099.
(37) Harriman, K. L. M.; Brosmer, J. L.; Ungur, L.; Diaconescu, P. L.; Murugesu, M. Pursuit of Record Breaking Energy Barriers: A Study of Magnetic Axiality in Diamide Ligated DyIII Single-Molecule Magnets. *J. Am. Chem. Soc.* **2017**, *139*, 1420−1423.
(38) Ungur, L.; Chibotaru, L. F. Magnetic anisotropy in the excited states of low symmetry lanthanide complexes. *Phys. Chem. Chem. Phys.* **2011**, *13*, 20086−20090.
(39) Lempicki, A.; Samelson, H.; Brecher, C. The europium ion in octacoordinate crystal fields: Symmetry, potentential, and level splittings. *J. Mol. Spectrosc.* **1968**, *27*, 375−401.
(40) Dante Gatteschi, C. B. *Introduction to Molecular Magnetism: From Transition Metals to Lanthanides*; Wiley VCH, 2015.
(41) Katoh, K.; Aizawa, Y.; Morita, T.; Breedlove, B. K.; Yamashita, M. Elucidation of Dual Magnetic Relaxation Processes in Dinuclear Dysprosium(III) Phthalocyaninato Triple-Decker Single-Molecule Magnets Depending on the Octacoordination Geometry. *Chem.−Eur. J.* **2017**, *23*, 15377−15386.
(42) Horii, Y.; Kishiue, S.; Damjanović, M.; Katoh, K.; Breedlove, B. K.; Enders, M.; Yamashita, M. Supramolecular Approach for Enhancing Single-Molecule Magnet Properties of Terbium(III)-Phthalocyaninato Double-Decker Complexes with Crown Moieties. *Chem. - Eur. J.* **2018**, *24*, 4320−4327.
(43) Komeda, T.; Katoh, K.; Yamashita, M. *Single Molecule Magnet for Quantum Information Process*; Molecular Technology, 2018, pp 263−304.
(44) Katoh, K.; Asano, R.; Miura, A.; Horii, Y.; Morita, T.; Breedlove, B. K.; Yamashita, M. Effect of f−f interactions on quantum tunnelling of the magnetization: mono- and dinuclear Dy(iii) phthalocyaninato triple-decker single-molecule magnets with the same octacoordination environment. *Dalton Trans.* **2014**, *43*, 7716−7725.
(45) Li, Q.-W.; Liu, J.-L.; Jia, J.-H.; Chen, Y.-C.; Liu, J.; Wang, L.-F.; Tong, M.-L. Half-sandwich″ YbIII single-ion magnets with metallacrowns. *Chem. Commun.* **2015**, *51*, 10291−10294.
(46) AlDamen, M. A.; Clemente-Juan, J. M.; Coronado, E.; Martí-Gastaldo, C.; Gaita-Ariño, A. Mononuclear Lanthanide Single-Molecule Magnets Based on Polyoxometalates. *J. Am. Chem. Soc.* **2008**, *130*, 8874−8875.
(47) Vonci, M.; Giansiracusa, M. J.; Gable, R. W.; Van den Heuvel, W.; Latham, K.; Moubaraki, B.; Murray, K. S.; Yu, D.; Mole, R. A.; Soncini, A.; et al. Ab initio calculations as a quantitative tool in the inelastic neutron scattering study of a single-molecule magnet analogue. *Chem. Commun.* **2016**, *52*, 2091−2094.
(48) Li, Q.-W.; Wan, R.-C.; Chen, Y.-C.; Liu, J.-L.; Wang, L.-F.; Jia, J.-H.; Chilton, N. F.; Tong, M.-L. Unprecedented hexagonal bipyramidal single-ion magnets based on metallacrowns. *Chem. Commun.* **2016**, *52*, 13365−13368.
(49) Li, J.; Gómez-Coca, S.; Dolinar, B. S.; Yang, L.; Yu, F.; Kong, M.; Zhang, Y.-Q.; Song, Y.; Dunbar, K. R. Hexagonal Bipyramidal Dy(III) Complexes as a Structural Archetype for Single-Molecule Magnets. *Inorg. Chem.* **2019**, *58*, 2610−2617.
(50) Zhao, W.; Cui, H.; Chen, X.-Y.; Yi, G.; Chen, L.; Yuan, A.; Luo, C.-L. An eight-coordinate ytterbium complex with a hexagonal bipyramid geometry exhibiting field-induced single-ion magnet behaviour. *Dalton Trans.* **2019**, *48*, 5621−5626.
(51) Bar, A. K.; Kalita, P.; Sutter, J.-P.; Chandrasekhar, V. Pentagonal-Bipyramid Ln(III) Complexes Exhibiting Single-Ion-Magnet Behavior: A Rational Synthetic Approach for a Rigid Equatorial Plane. *Inorg. Chem.* **2018**, *57*, 2398−2401.
(52) Kalita, P.; Ahmed, N.; Bar, A. K.; Dey, S.; Jana, A.; Rajaraman, G.; Sutter, J.-P.; Chandrasekhar, V. Pentagonal Bipyramidal Ln(III) Complexes Containing an Axial Phosphine Oxide Ligand: Field-induced Single-ion Magnetism Behavior of the Dy(III) Analogues. *Inorg. Chem.* **2020**, *59*, 6603−6612.
(53) Alvarez, S.; Alemany, P.; Casanova, D.; Cirera, J.; Llunell, M.; Avnir, D. Shape maps and polyhedral interconversion paths in transition metal chemistry. *Coord. Chem. Rev.* **2005**, *249*, 1693−1708.
(54) Casanova, D.; Alemany, P.; Bofill, J. M.; Alvarez, S. Shape and Symmetry of Heptacoordinate Transition-Metal Complexes: Structural Trends. *Chem. - Eur. J.* **2003**, *9*, 1281−1295.
(55) Pinsky, M.; Avnir, D. Continuous Symmetry Measures. 5. The Classical Polyhedra. *Inorg. Chem.* **1998**, *37*, 5575−5582.
(56) Casanova, D.; Cirera, J.; Llunell, M.; Alemany, P.; Avnir, D.; Alvarez, S. Minimal Distortion Pathways in Polyhedral Rearrangements. *J. Am. Chem. Soc.* **2004**, *126*, 1755−1763.
(57) Cirera, J.; Ruiz, E.; Alvarez, S. Shape and Spin State in Four-Coordinate Transition-Metal Complexes: The Case of the d6 Configuration. *Chem. - Eur. J.* **2006**, *12*, 3162−3167.
(58) Chilton, N. F.; Collison, D.; McInnes, E. J. L.; Winpenny, R. E. P.; Soncini, A. An electrostatic model for the determination of magnetic anisotropy in dysprosium complexes. *Nat. Commun.* **2013**, *4*, 2551.
(59) Chen, G.-J.; Gao, C.-Y.; Tian, J.-L.; Tang, J.; Gu, W.; Liu, X.; Yan, S.-P.; Liao, D.-Z.; Cheng, P. Coordination-perturbed single-molecule magnet behaviour of mononuclear dysprosium complexes. *Dalton Trans.* **2011**, *40*, 5579−5583.
(60) Chilton, N. F.; Langley, S. K.; Moubaraki, B.; Soncini, A.; Batten, S. R.; Murray, K. S. Single molecule magnetism in a family of mononuclear β-diketonate lanthanide(III) complexes: rationalization of magnetic anisotropy in complexes of low symmetry. *Chem. Sci.* **2013**, *4*, 1719−1730.
(61) Giordano, T. J.; Palenik, G. J.; Palenik, R. C.; Sullivan, D. A. Pentagonal-Bipyramidal Complexes. Synthesis and Characterization of Aqua(nitrato)[2,6-diacetylpyridinebis(benzoic acid hydrazone)]-cobalt(II) Nitrate and Diaqua[2,6-diacetylpyridinebis(benzoic acid hydrazone)]nickel(II) Nitrate Dihydrate. *Inorg. Chem.* **1979**, *18*, 2445.
(62) Dubován, L.; Pöllnitz, A.; Silvestru, C. Tri(3-pyridyl)- and Tri(4-pyridyl)phosphine Chalcogenides and Their Complexes with ZnTPP (TPP = Tetraphenylporphyrinate). *Eur. J. Inorg. Chem.* **2016**, *2016* (10), 1521−1527.
(63) International Tables for Crystallography.
(64) Kahn, O. *Molecular Magnetism*; VCH: Weinheim, 1993.
(65) Chilton, N. F.; Anderson, R. P.; Turner, L. D.; Soncini, A.; Murray, K. S. A powerful new program for the analysis of anisotropic monomeric and exchange-coupled polynuclear d- and f-block complexes. *J. Comput. Chem.* **2013**, *34*, 1164.

https://doi.org/10.1021/acsomega.2c03631
ACS Omega 2022, 7, 25881−25890